Journal of Catalysis 335 (2016) 36–46

Contents lists available at ScienceDirect

Journal of Catalysis

journal homepage: www.elsevier.com/locate/jcat

Effect of activation atmosphere in the Fischer–Tropsch Synthesis using a "quasi-model" catalyst of γ-Fe_2O_3 nanoparticles supported on SBA-15

Ignacio O. Pérez De Berti [a], José F. Bengoa [a], Silvana J. Stewart [b,c], María V. Cagnoli [a], Gina Pecchi [d], Sergio G. Marchetti [a,*]

[a] CINDECA, CONICET-CICPBA-Universidad Nacional de La Plata, Facultad de Ciencias Exactas, Calle 47 N 257, 1900 La Plata, Argentina
[b] IFLP-CCT-La Plata-CONICET and Departamento de Física, Facultad de Ciencias Exactas, C. C. 67, Universidad Nacional de La Plata, 1900 La Plata, Argentina
[c] Instituto Ciencias de la Salud, Universidad Nacional Arturo Jauretche, Avenida Calchaquí N° 6200, Florencio Varela, Argentina
[d] Departamento de Físico Química, Facultad de Ciencias Químicas, Universidad de Concepción, Casilla 160-C, Concepción, Chile

ARTICLE INFO

Article history:
Received 6 November 2015
Revised 10 December 2015
Accepted 12 December 2015
Available online 11 January 2016

Keywords:
"Quasi-model" catalysts
Iron oxides nanoparticles
Fischer–Tropsch Synthesis
Fe/SBA-15 system
Activation atmosphere effect
Mössbauer spectroscopy

ABSTRACT

The effect of different activation atmospheres ($CO:H_2$ or pure H_2) on activity and selectivity of iron nanoparticles supported on SBA-15 in Fischer–Tropsch Synthesis, has been studied. To achieve this aim a new preparation method, using monodisperse pre-synthesized γ-Fe_2O_3 nanoparticles of 3 nm size, supported on SBA-15, was used. These catalysts have structural properties between real and model catalysts. Therefore, they were named "quasi-model" catalysts. Nanoparticles and catalysts were characterized with several techniques: XRD, N_2 adsorption at 77 K, magnetic measurements, electron transmission microscopy, Mössbauer spectroscopy between 298 and 13 K in air and controlled atmosphere and thermal gravimetric analysis. Catalytic tests showed clearly that activation with pure H_2 leads to a catalyst more active and less selective to methane than that activated with $CO:H_2$. To explain these results, different reduction steps were proposed. These different sequences would produce a diverse number of active sites.

1. Introduction

The Fischer–Tropsch Synthesis (FTS) is a widely known process, used to produce hydrocarbons from syngas (a mixture of H_2 and CO) [1,2]. It can be schematized in the following way:

$$(2n+1)H_2 + nCO \rightarrow C_nH_{2n+2} + nH_2O$$

Different metals are active as catalysts in FTS but, up to the present, Co and Fe are the only reasonable commercial catalysts for this process [3]. This article will be focused on iron catalysts. The technological process can be considered as "mature", since the first patent appeared in 1913 and in 1938 had various industrial plants in operation [4]. However, nowadays many doubts about these kinds of catalysts remain without solution. As a consequence of the complex composition of "working" catalyst, it is very hard to determine a correlation between the catalyst composition and its activity and selectivity [5–7]. The active sites and the mechanism of the reaction remain unclear [5–15] and the best activation treatment is under discussion too [4,16–20]. Besides, the FTS would be "structure sensitive" [21–24], but more studies are necessary to confirm this property. Additional difficulties appear when promoters are added.

These ambiguous situations arise considering that more than one variable is changed when the studies are realized. In order to overcome this situation, model catalysts can be used. They can be prepared using pure nanoparticles (NPs), with adjustable size and a very narrow size distribution. These systems would avoid a misunderstanding of the results. However, the methods to obtain the model catalysts are complex, and NPs are on planar supports of thin oxide films [25]. These flat surfaces have very different properties compared with the actual catalyst. The real catalysts have pores, which can provide diffusional hindrance and/or shape selectivity.

In recent years, synthesis methodologies of Fe oxide nanoparticles (NPs) with very narrow size distributions have been published [26,27]. These results open new possibilities to synthesize "tailored" catalysts. Thus, in the present work, we report a new synthesis method to obtain Fe catalysts for FTS with the aim of overcoming the difficulties previously mentioned. The solid was prepared embedding pre-synthesized Fe oxide NPs, with a narrow particle size distribution, inside the pores of a suitable mesoporous support as SBA-15. The selected support has a narrow pore-size

* Corresponding author.
E-mail address: march@quimica.unlp.edu.ar (S.G. Marchetti).

http://dx.doi.org/10.1016/j.jcat.2015.12.004
0021-9517/

distribution and thermal stability. Besides, the pore diameters can be tailored to locate the iron NPs inside them [28,29]. This system will be called "quasi-model catalyst" since it has properties of a model catalyst (very narrow size distribution of the active phase) and of an actual catalyst (the support has pores and the NPs are inside them). Up to our knowledge this is the first time that this synthesis methodology is reported. Researchers of University of Cape Town described for the first time the preparation of supported iron catalysts to be used in the FTS using iron oxide NPs pre-synthesized. They contacted these NPs with two amorphous supports: Al_2O_3 and carbon [30,31]. However, only NPs with sizes between 3 and 7 nm are able to be located inside the Al_2O_3 pores. The other NPs are on the support external surface. Besides, the authors detected the appearance of NPs agglomerates. This result would be indicative of sintering of a NPs fraction. Afterward, Fe/Al_2O_3 catalysts were obtained by Park et al. [32]. They used pre-synthesized NPs of γ-Fe_2O_3 supported on δ-Al_2O_3. But these authors did not discuss whether these NPs are inside or outside of the support pores.

The aim of the present article was to study the effect of the activation method on the activity and selectivity in the FTS using a "quasi-model catalyst" of iron oxide NPs with 3 nm diameter located inside SBA-15 pores. This system would allow studying this effect without the influence of the other variables previously mentioned.

2. Experimental section

The syntheses were carried out using commercially available reagents. Diphenyl ether (99%), oleic acid (90%), oleylamine (>70%), iron (III) acetylacetonate (97%) ($Fe(acac)_3$) and tetraethyl orthosilicate (TEOS) were purchased from Aldrich Chemical Co., Pluronic triblock copolymer P_{123} (EO_{20}-PO_{70}-EO_{20}) from BASF, cyclohexane (99.5%) (CH) from Carlo Erba and NH_4F (98%) from Riedel de Haën. These reactants, ethanol and hexane, were used as they were received.

2.1. Synthesis of iron oxide NPs

The methodology proposed by Perez De Berti et al. [27] was followed to produce 3 nm γ-Fe_2O_3 NPs. Thus, $Fe(acac)_3$ (4 mmol), oleic acid (12 mmol), oleylamine (12 mmol), and diphenyl ether (20 ml, boiling point: 532 K) were mixed and magnetically stirred under air. The mixture was heated at 473 K for 45 min and then heated to reflux (532 K) for another 45 min. The black–brown mixture was cooled at room temperature. Under ambient conditions, ethanol (80 ml) was added to the mixture, and a black–brown material was precipitated and separated via centrifugation. The product was dispersed in hexane in the presence of oleic acid as surfactant (0.1 ml) and oleylamine (0.1 ml). Centrifugation (6000 rpm, 10 min) was applied to remove any un-dispersed residue. The product, was then precipitated with ethanol, centrifuged (6000 rpm, 10 min) to remove the solvent, and re-dispersed into hexane.

2.2. Synthesis of mesoporous SBA-15 support

The SBA-15 support was synthesized according to the methodology proposed by Zhao et al. [28,29,33] modified by the addition of co-solvent to increase the pore size. The SBA-15 was synthesized using P_{123} as organic structure-directing agent, TEOS as silica source and CH as a "swelling" agent of the micelle. The molar composition of the synthesis mixture was as follows: $TEOS:P_{123}:CH:NH_4F:HCl:H_2O$ = 1:0.0168:0.199:0.0295:4.42:186. Pluronic and NH_4F were dissolved in HCl [1.3 M]. The mixture was transferred to a beaker and immersed into a thermostatic bath at 287 K with mechanical stirring for 1 h. TEOS and CH were added and the mix was kept into the bath with stirring for 24 h. The gel was heated at 373 K for 2 days into a Teflon lined autoclave. The solid product was recovered by filtering, washing with ethanol/H_2O 1:1, and calcining in air flow from room temperature to 823 K (2 K/min; Q_{air} = 150 cm^3/min) and was kept at this temperature for 5 h to remove the surfactant.

2.3. Catalyst preparation

Initially, dry SBA-15 was immersed in pure hexane during 10 min, in order to fill the channels with solvent. Then, the suspension of the NPs in hexane, required to get 15% w/w of nominal Fe concentration, was added. Next, all the solvent was removed slowly in a rotary evaporator with vacuum at 333 K. The different NPs concentration between suspension and SBA-15 channels produces the "driving force" to introduce the NPs inside the porous of the support. This dry solid was called precursor p-Fe/SBA-15. It was split in two fractions, which were activated "in situ" inside a stainless steel fixed-bed reactor (2.54 cm o.d.). Both were heated in N_2 flow from room temperature to 523 K (10 K/min; Q_{N2} = 150 cm^3/min), kept at this temperature for 1 h to remove the oleic acid surfactant coverage (as it will be explained below) and then cooled at room temperature ("peel-off" treatment). These variables were selected from the TGA results. After this treatment, each solid was activated "in situ" inside this reactor in the following conditions:

- one of these fractions was heated in a premixture of $CO:2H_2$ stored in a cylinder (10 K/min, $Q_{CO:2H2}$ = 20 cm^3/min) up to 603 K and atmospheric pressure. When this temperature was reached, the heating was turned-off and the solid was cooled "in situ" under $CO:2H_2$ mixture flow up to 298 K. In this way, the fresh activated catalyst was obtained. It was called c-CO:H_2-Fe/SBA-15,
- the second fraction was heated in pure H_2 (10 K/min, Q_{H2} = 60 - cm^3/min) at atmospheric pressure up to 688 K. When this temperature was reached, the heating was turned-off and the solid was cooled "in situ" to 298 K under H_2 flow. This fresh catalyst was named c-H_2-Fe/SBA-15.

In order to select the operative activation conditions we considered the following topics:

- produce the maghemite reduction into one or both iron species commonly found in the Fischer–Tropsch reaction conditions: magnetite and/or iron carbides,
- use minimum temperature to produce this reduction to avoid any sintering possibility, and
- hinder the carbon monoxide disproportionation in order to avoid a possible carbon deposition.

Bearing in mind these considerations and the fact that CO reduction power is higher than that of H_2 (e.g. see curve $4Fe_3O_4 + O_2 \rightarrow 6Fe_2O_3$ in the temperature range between 600 and 700 K in Ellingham diagram), we selected 603 K for H_2:CO mixture and 688 K for pure H_2 as the maxima activation temperatures. At temperatures higher than 603–623 K carbon deposition could begin when H_2:CO mixture is used. On the other hand, due to the lower hydrogen reduction power, temperatures lower than 673–723 K do not produce the maghemite reduction to magnetite [34] (we verified this temperature by TPR). For these reasons different maxima activation temperatures were selected. We prefer select these temperatures since the effects of the different activation atmospheres can be seen without any of the interferences previously mentioned.

The same activation treatments were repeated in a cell specially built by our group with the aim to characterize the fresh catalyst in the same activation atmosphere by Mössbauer spectroscopy [35].

2.4. Catalytic tests

Catalytic tests were carried out after activation treatments pressurizing "in situ" up to 20 atm and heated from 298 to 603 K under 20 cm^3/min $CO:2H_2$ of total flow. When these conditions were reached, zero reaction time was considered. In order to produce a space velocity of 828 h^{-1}, 130 mg of catalyst (diluted with 270 mg of SBA-15) was used. The catalytic tests were carried out during 60 h.

All gases were passed through the following filtering elements (at RT): a Mn-based catalyst to remove residual O_2 (All-pure trap, Alltech) and a molecular sieve 5A to remove water traces. In addition, the mixture $CO:2H_2$ was passed through a filter (heated at 353 K) to remove some Fe or Ni carbonyl compounds that could be produced in the gas bottle and the flow lines. All gas flows were measured and controlled by mass flow meters (Sierra Inst Smart Track). The reaction products were analyzed online by gas chromatography using FID and TCD detectors with a GS-Gas Pro capillary column and a HAYESEP DB 100/120 packed, respectively. After reactor, the tubing lines were kept at about 503 K to avoid product condensation. Under these reaction conditions, heavy hydrocarbons and waxes were produced. Therefore, a cold trap to collect these fractions was necessary in order to analyze hydrocarbons from methane to C_{13}. The capillary column selected is adequate to analyze the hydrocarbon fraction (olefins and paraffins) up to this carbon number. Taking into account that this trap is located after the back pressure of the equipment, its temperature was fixed through an estimation of the "dew point" of the heavy hydrocarbon fraction at one atmosphere. Downstream the trap, the products went through a six-way injection valve that collected 1.8 cm^3 of gas sample to be injected into the capillary column for hydrocarbons using a split ratio of 20:1 or through a second six-way valve, to inject permanent gases into the packed column. Also, it was determined that the stainless steel reactor was inactive for reaction under the test conditions, when it is used without catalyst.

In order to obtain the Mössbauer spectra to determine the iron species and structural properties of the "working" catalysts at 20 atm, after 48 h of FTS, the system was cooled in synthesis gas stream, and the reactor was isolated in the same atmosphere and transferred to a glove box. Air and moisture were removed from the box with Ar flow during 48 h (Q_{Ar} = 120 cm^3/min) to prevent re-oxidation of the used catalysts. Then, the samples were transferred into an airtight cell previously described [35]. The used catalysts were called us-$CO:H_2$-Fe/SBA-15 and us-H_2-Fe/SBA-15.

2.5. Catalyst characterization

The samples were characterized by chemical analysis, X-ray diffraction (XRD) at low angles, N_2 adsorption at 77 K, Mössbauer spectroscopy (MS) between 298 and 13 K in air and controlled atmosphere, Transmission Electron Microscopy (TEM), Magnetic measurements (M vs. H and Zero Field Cooling–Field Cooling (ZFC–FC)) and Thermal Gravimetric Analysis (TGA).

The Fe content of p-Fe/SBA-15 was determined using a modification of a colorimetric method using Perkin–Elmer Lambda 35. First, the sample was calcined with a burner. Then it was attacked with HCl/HF mixture up to complete dissolution and after that was treated according to conventional methods for this technique [36].

The X-ray diffraction patterns at low angles were performed in the D11A-SAXS beamline at the Brazilian Synchrotron Light Laboratory. All data were registered at 300 K using 300k Pilatus bidimensional detector at a wavelength λ = 1.488 A.

Textural properties, specific surface area (S_g), specific pore volume (V_p) and pore diameter (D_p), were measured in a Micromeritics equipment ASAP 2020 V1.02 E with N_2 at 77 K.

NPs for TEM analysis were prepared drying the dispersion on amorphous carbon coated copper grids. TEM micrographs were obtained on a JEOL model JEM-1200 EX II microscope. The same procedure was applied with the precursor. Measures with dark field were done too.

The magnetic measurements were carried out using a Multipurpose Physical Magnetic System (MPMS) superconducting quantum interference device (SQUID) from Quantum Design. The magnetization versus magnetic field (M–H) curves were recorded at 5 and 300 K up to a maximum magnetic field of 50 kOe. Thermal dependences of the magnetization under zero field cooling (ZFC) and field cooling (FC) conditions were recorded using an external field of 50 Oe. Combining the iron loading of the sample (determined by colorimetric method previously described) with the mass used in each measurement, all magnetic results can be normalized by iron oxide mass.

The Mössbauer spectra were obtained in transmission geometry with a 512-channel constant acceleration spectrometer. A source of ^{57}Co in Rh matrix of nominally 50 mCi was used. Velocity calibration was performed against a 12-μm-thick α-Fe foil. All isomer shifts (δ) mentioned in this paper are referred to this standard. Temperature was varied between 13 and 298 K working with an ARS closed-cycle cryogenic system. The Mössbauer spectra were evaluated using a commercial program with constraints named Recoil [37]. Although some spectra display magnetic relaxation, for simplicity, Lorentzian lines with equal widths were considered for each spectrum component. The spectra were folded to minimize geometric effects. The spectra of the activated and used samples were obtained in their corresponding atmospheres, using a cell specially built by us with this purpose, to be used inside the cryogenic system [35].

The TGA measurements were performed on a Shimadzu TGA-50 equipment. The sample was heated from room temperature up to 1023 K at a heating rate of 5 K/min under air flow (20 cm^3/min).

3. Results

3.1. NPs characterization

TEM analysis shows that NPs have a very narrow size distribution. Fig. 1 displays typical TEM image from a representative sample. We observed that the particles have nearly spherical shape.

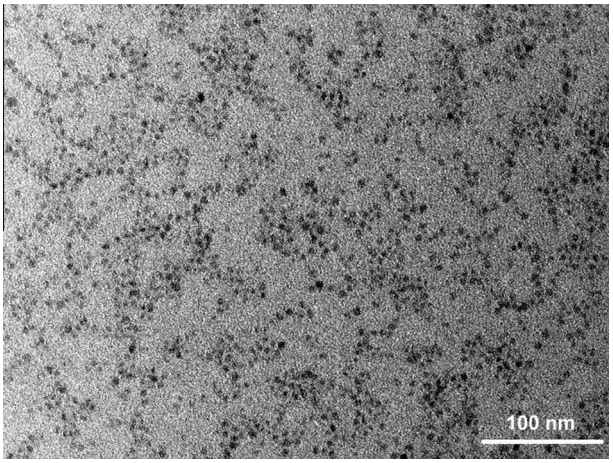

Fig. 1. Representative TEM image of NPs.

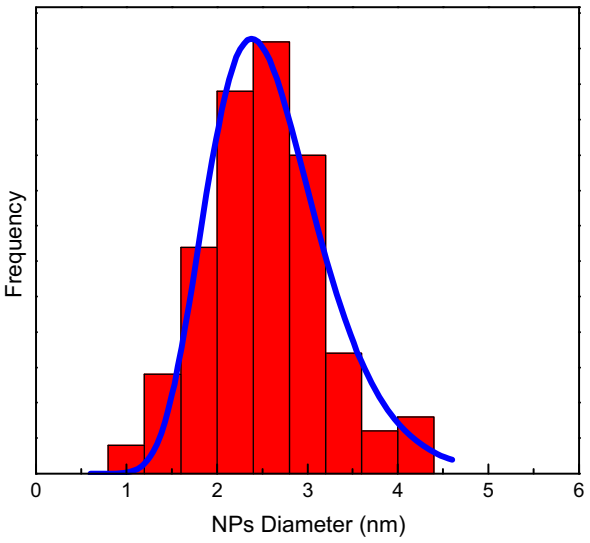

Fig. 2. Size distributions of NPs from TEM measurements. Solid (blue) line was obtained fitting the results by assuming a log-normal distribution.

Fig. 2 shows the histogram obtained counting 320 NPs. It was fitted using a log-normal distribution, in agreement with previous studies that shown that particles lower than 20 nm present this type of distribution [38]. The obtained statistical parameters are geometric average (μ_g) = 3 nm and geometric standard deviation (σ_g) = 1 nm. It is important to remark that 97% of the NPs population is included between $\pm\sigma_g$. Therefore, it can be considered that we have obtained a monodisperse size distribution.

In order to identify the iron species of the NPs, Mössbauer spectra were acquired at 298, 30 and 13 K. The spectra are shown in Fig. 3 and their hyperfine parameters are displayed in Supplementary Data section (Table I). At 13 K, the spectrum shows six broad lines with a curved background. These characteristics are typical of a sample with a partial magnetic blocking. This spectrum was fitted with two sextuplets: one of them magnetically blocked and the other one relaxing. Besides, a central doublet was necessary to achieve a good fitting. Both sextuplets have hyperfine parameters typical of γ-Fe_2O_3 [39] but the relaxing effect did not allow to distinguish between Fe^{3+} ions located in tetrahedral (A) and octahedral (B) sites. The presence of Fe^{2+} ions was not detected. From the above results, the existence of Fe_3O_4 was discarded. The central doublet at 13 K can hardly be assigned to γ-Fe_2O_3 with sizes smaller than 3 nm. Indeed, it will be expected that NPs with sizes between 2 and 3 nm (the lower range of the size distribution) would be partially blocked taking into account the large anisotropy constant of about 2×10^3 J m^{-3} [40]. Recently, it had been found, by FTIR, that surface Fe^{3+} ions can be complexed with oleic acid (the surfactant used in the NPs synthesis) through carboxylate heads with monodentate and bidentate coordination [35,41,42]. Therefore, this doublet was assigned to this complex. It is important to remark that the isomer shift of the doublet is small (δ = 0.2 ± 0.1 mm s^{-1}) in comparison with the typical values of high spin Fe^{3+} ions at low temperature (about 0.4–0.5 mm s^{-1}). This result would indicate an increase of the covalence of the iron bond in the presence of carboxylate ligands (an increase of 4 s electron density in the iron nucleus). When the temperature is increased from 13 to 30 K the relaxing fraction is increased. Finally, at 298 K a maghemite fraction begins the magnetic blocking and the remaining fraction is in a complete superparamagnetic regime (SP). For this reason, the doublet area at 298 K is higher than that at lower temperatures: this doublet arises from the areas addition of γ-Fe_2O_3 (SP) NPs and surface Fe^{3+} ions coordinated with oleic acid.

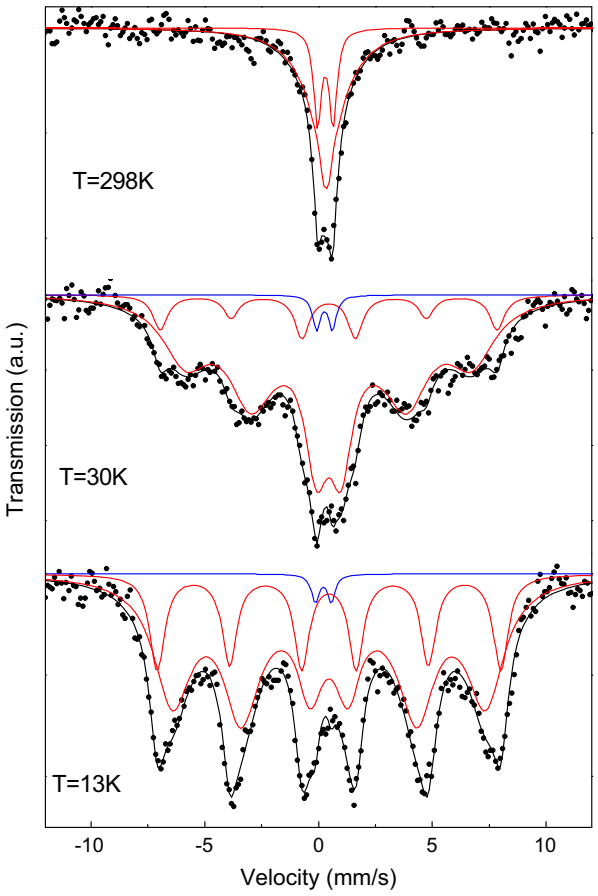

Fig. 3. Mössbauer spectra of NPs at 298, 30 and 13 K.

In Fig. 4a M vs. H curves at 298 and 5 K can be seen. At 298 K the absence of M vs. H hysteresis loop is typical of superparamagnetic NPs in agreement with Mössbauer results. At 5 K, remanence (M_r) and coercitive field (H_c) values are very small (6 emu g^{-1} Fe_2O_3 and 91 Oe respectively). Therefore, the magnetic blocking is not complete. The saturation magnetization (M_s) at this temperature is of 44 emu g^{-1} Fe_2O_3, and this value is about 41% lower than the bulk one (about 74 emu g^{-1} Fe_2O_3 [43]). This effect has been usually reported in magnetic small particles. The first study of M_s decrease in γ-Fe_2O_3 NPs was reported by Coey [44]. This author showed that this decrease is due to the existence of non-collinear spins at the surface of the particles.

ZFC and FC magnetization curves of NPs are shown in Fig. 4b. The behavior of ZFC curve is typical of superparamagnetic NPs arrangement, whose magnetization increases when the temperature increases up to a maximum value (T_{max} = 17 K). At higher temperatures, the decrease of the magnetization is the predominant effect. The FC and ZFC curves split below a temperature called the irreversibility temperature (T_{irr}), which is associated with the blocking of the largest particles. We consider T_{irr} as the temperature where the difference between FC and ZFC curves, normalized to FC maximum value at T = 4 K, becomes smaller than 3% [45,46]. For this sample, T_{irr} = 35 K. The difference between T_{irr} and T_{max} provides a measure of the width of the blocking temperature distribution and in consequence of the particle size distribution, assuming the same anisotropy constant and the absence of interparticle interactions. In the present sample, $T_{irr} - T_{max}$ = 18 K, this value would confirm the existence of a narrow size distribution. The present result is in agreement with TEM results. On the other hand, the FC curve shows a continuous increase of the magnetization

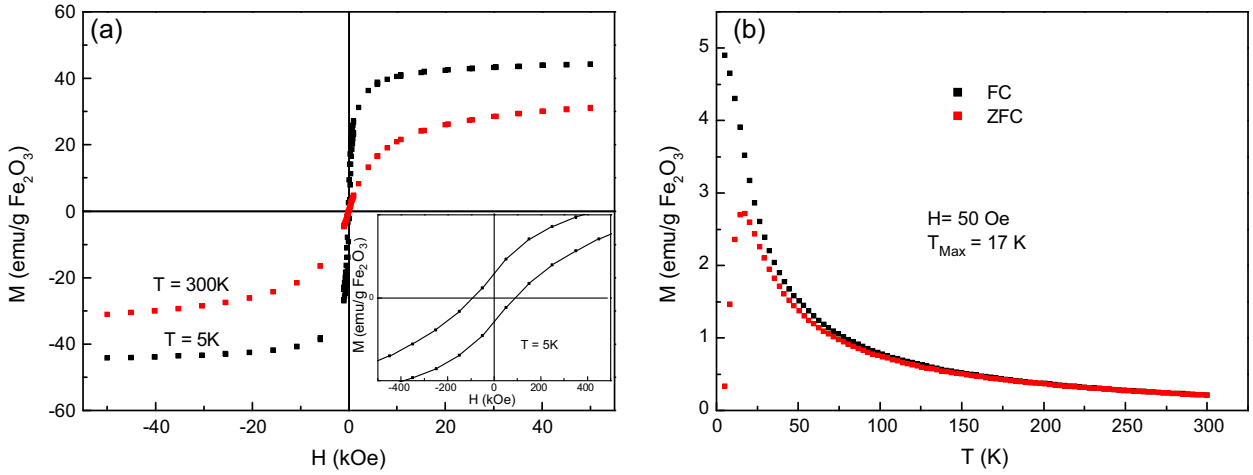

Fig. 4. (a) *M* versus *H* loops at 300 and 5 K for NPs. The inset shows the remanence and coercivity at 5 K. (b) ZFC–FC magnetization curves for NPs.

when the temperature decreases in the presence of small external magnetic field. This behavior displays that there is no interaction between the NPs. Finally, the coincidence of ZFC–FC curves after the maximum value of ZFC is another proof of the superparamagnetism of the NPs.

In order to determine the temperature of surfactant elimination from NPs surface, a TGA was done. Fig. 5 displays that at 543 K the higher velocity of surfactant elimination was reached.

3.2. SBA-15 characterization

The ordered hexagonal structure of mesoporous SBA-15, used as support, was verified by XRD (Fig. 6), and TEM micrographs (Fig. 7). Besides, textural properties are characteristic of this kind of solids: $S_g = 420\ m^2\ g^{-1}$, $V_p = 1.1\ cm^3\ g^{-1}$, $D_p = 9$ nm and wall thickness of 2.8 nm.

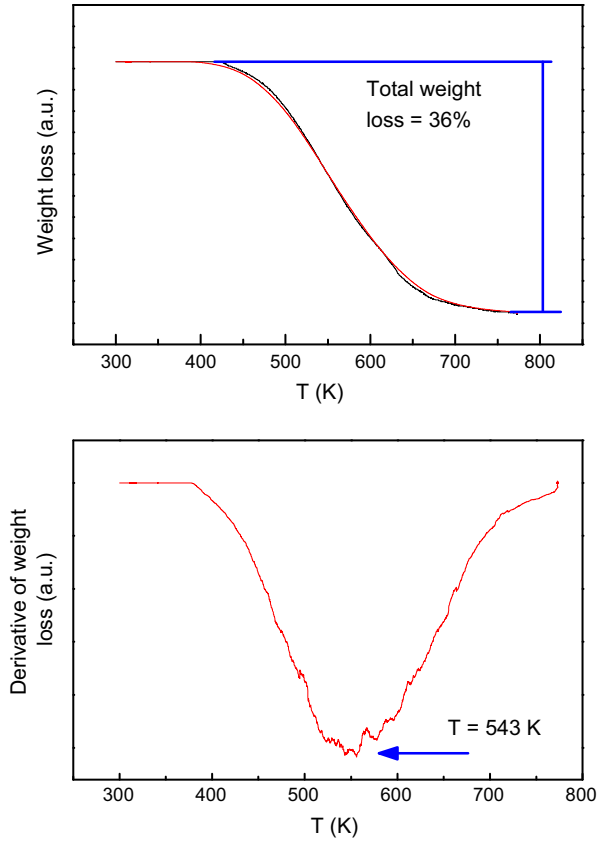

Fig. 5. The TG/DTG curves of NPs.

3.3. Precursor characterization

The impregnation treatment, which leads to obtain p-Fe/SBA-15, did not change the structural properties of the mesoporous support, as it was verified by XRD and TEM techniques (Figs. 6 and 8). The intensity differences between diffractograms of SBA-15 and p-Fe/SBA-15 are produced by changes in the energy of the synchrotron beam. In Fig. 8 small dark points inside the channels (light areas) could be ascribed to NPs. Besides, analyzing dark field TEM micrograph (Fig. 9), it can be seen that bright points assignable to NPs are aligned following the channels path.

With the aim of reinforcing this conclusion an indirect result could be considered. Thus, after impregnation, surface area decreases from 420 to 258 m^2/g and pore volume from 1.1 to 0.9 cm^3/g. These results are obtained with a bulk technique, and in consequence, are not circumscribed at the small areas analyzed with TEM. Nominal Fe loading was 15% wt/wt.

Curves of *M* vs. *H* and ZFC–FC for p-Fe/SBA-15 (not shown) were nearly equal to those of the isolated NPs. Considering that, as it was

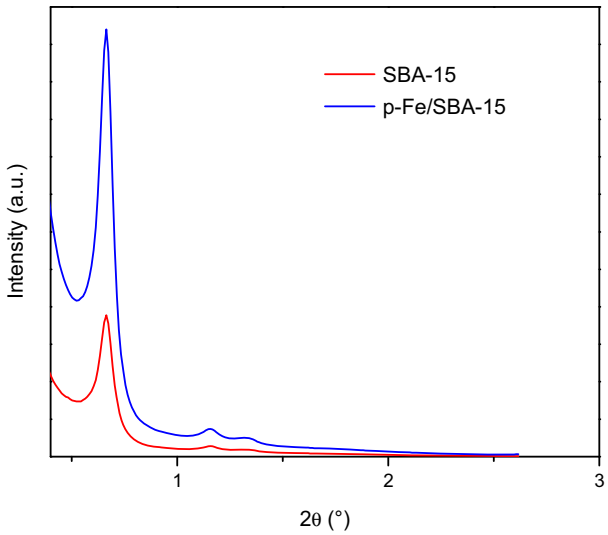

Fig. 6. XRD diffractograms of SBA-15 and p-Fe/SBA-15.

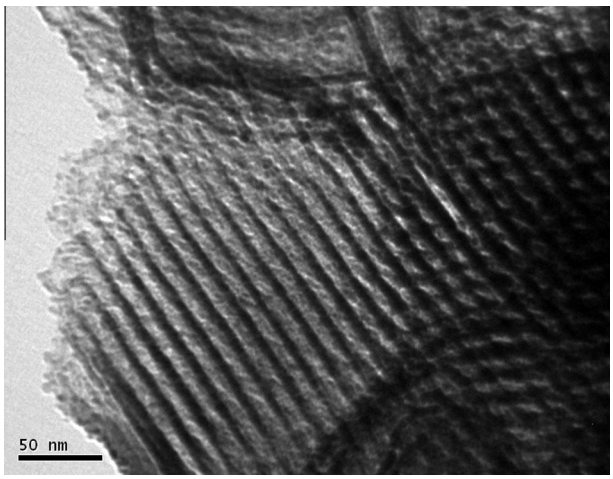

Fig. 7. TEM image of SBA-15.

previously described, a continuous increase of the magnetization in FC curve displays that there is no interaction between the NPs, it can be inferred that NPs did not suffer agglomeration after impregnation. Mössbauer spectra and hyperfine parameters of p-Fe/SBA-15 at 298, 30 and 13 K (not shown) were nearly indistinguishable from those obtained with isolated nanoparticles. This is other evidence, using an independent technique, that the impregnation process on SBA-15 support did not affect the properties of the original NPs.

3.4. Activated catalysts characterization

Fig. 10a displays the Mössbauer spectra of c-CO:H_2-Fe/SBA-15 at 298 and 13 K after "peel-off" and activation treatments measured in controlled atmosphere and the hyperfine parameters obtained with the fitting process are shown in Supplementary Data (Table II).

The precursor activated in CO:H_2 showed the principal signals in the center of the spectrum at 298 K. They could be assigned to superparamagnetic and/or paramagnetic species (distinction between both species will arise in the Mössbauer spectrum at 13 K). Besides, very small magnetic signals with low hyperfine fields can be distinguished. The fitting was made using two singlets, one doublet and two sextets. According to the description of Rancourt and Daniels [47], the singlets can be assigned to superparamagnetic Fe_3O_4. The doublet, can be attributed to Fe^{2+} ions diffused inside the walls of SBA-15 located into octahedral sites of SiO_2 [48]. Finally, the presence of two sextets with small intensity and low hyperfine fields can be ascribed to I and III crystallographic sites of χ-Fe_5C_2 [49]. The absence of iron oxide species magnetically blocked at 298 K would indicate that the activation process at 603 K did not produce sintering of the original NPs. We attribute this result to the great distance between the NPs (produced by the high specific surface area of the support) and the "anchoring" of the NPs generated by the Fe^{2+} ions diffusion into the walls of SBA-15. The presence of iron carbide sextuplets at 298 K is not in conflict with the previous conclusion. Taking into account that the effective magnetic anisotropy constant of iron carbides NPs is about two magnitude orders larger than that of iron oxides NPs ($\cong 2 \times 10^3$ J m^{-3} for maghemite NPs of 5 nm vs. $\cong 1$–1.2×10^5 J m^{-3} for $Fe_{2.2}C$ NPs of 12 mn) [40,50] the blocking temperature of iron carbides will result in higher than that of iron oxides NPs.

At 13 K, the spectrum is nearly completely blocked (six peaks can be seen). In order to fit this spectrum, one doublet and eight sextuplets were necessary. The doublet, belongs to Fe^{2+} ions diffused into the octahedral sites of SiO_2. Six sextuplets have hyperfine parameters assignable to different crystallographic sites of Fe_3O_4 NPs at low temperature [51]. Therefore, the central singlets, detected at room temperature and assigned to Fe_3O_4, have completely disappeared and they were replaced by these sextuplets. This experimental result confirms that, at room temperature, this species is in a complete superparamagnetic regime and it can be inferred that the activation process did not produce sintering. Finally, another two sextuplets were assignable to I and III sites of χ-Fe_5C_2 [49] and ε'-$Fe_{2.2}C$ sites [52]. Instead, at 298 K, only I and III sites of the χ carbide were detected. These results can be explained taking into account the extreme complexity and the strong overlapping of these sextuplets in the central region of the spectrum at 13 K. Therefore, there is a degree of uncertainty of the different sites percentages, but the error in the total content of iron carbides has an acceptable value considering these difficulties.

The spectrum of c-H_2-Fe/SBA-15 at 298 K, only showed a central signal assigned to superparamagnetic and/or paramagnetic species. Obviously, any magnetic signal corresponding to iron carbides

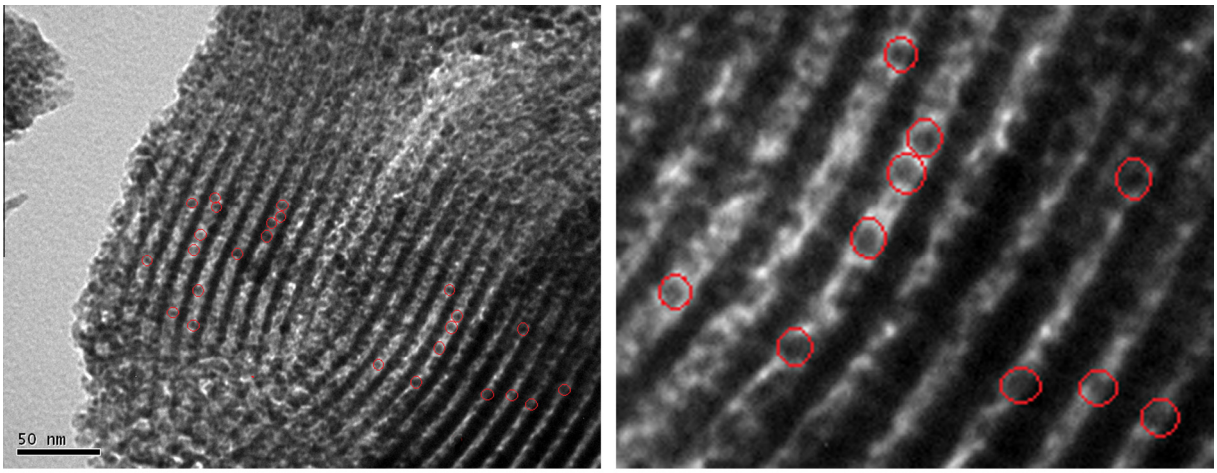

Fig. 8. (a) Light areas correspond to SBA-15 channels. Inside them, the small dark points could be ascribed to NPs (some of them are marked with red circles). All of them have a size of about 3 nm. (b) An enlargement of one section of this photograph is shown.

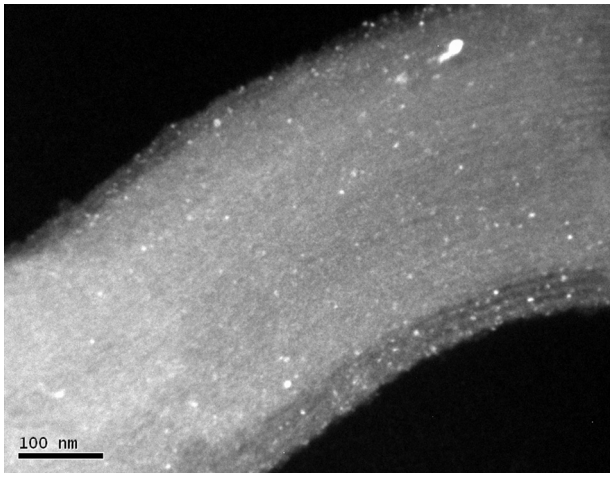

Fig. 9. Dark-field image of p-Fe/SBA-15.

was detected. In order to get the fitting, we use two singlets and two doublets (Fig. 10b and Supplementary Data (Table III)). In the same way that c-CO:H_2-Fe/SBA-15 the singlets were assigned to superparamagnetic Fe_3O_4 (it will be corroborated with the measurement at 13 K). Doublets were ascribed to Fe^{2+} diffused into octahedral and tetrahedral sites of SiO_2. In comparison with c-CO:H_2-Fe/SBA-15, in this catalyst it is possible to detect the Fe^{2+} ions, located in both sites, since their percentage is larger.

At 13 K, appear some differences in comparison with c-CO:H_2-Fe/SBA-15. Again, the singlets completely disappear and they were replaced by magnetic signals with hyperfine parameters typical of Fe_3O_4. Therefore, once more the singlets at 298 K, belong to superparamagnetic Fe_3O_4 and, in the same way that c-CO:H_2-Fe/SBA-15, sintering can be discarded. Notwithstanding, these magnetic signals did not complete their blocking at 13 K and this situation did not allow us to distinguish the six different crystallographic sites. This behavior would suggest that Fe_3O_4 NPs in this catalyst have lower size than in c-CO:H_2-Fe/SBA-15. As it will be explained below, iron carbides, detected in c-CO:H_2-Fe/SBA-15, would produce a "shell" on Fe_3O_4 surface. When two different magnetic systems are in intimate contact, exchange anisotropy appears [53,54]. As it was previously explained, the anisotropy constant of iron carbides is about two magnitude orders larger than the iron oxides. Therefore, this fact would increase the magnetic anisotropy of Fe_3O_4 due to a magnetic exchange coupling between surface atoms belonging to both species. As a consequence, Fe_3O_4 NPs of c-CO:H_2-Fe/SBA-15 are magnetically blocked at higher temperature than c-H_2-Fe/SBA-15.

Table 1 displays the percentages of the different iron species. Within the experimental errors, both catalysts have the same percentage of Fe_3O_4. Obviously, in c-H_2-Fe/SBA-15, iron carbides were not detected since this catalyst was not in contact with CO. Besides, in this catalyst a higher percentage of Fe^{2+} ions diffused inside the SBA-15 walls were found.

3.5. Used catalysts characterization

The Mössbauer spectra of both used catalysts, us-CO:H_2-Fe/SBA-15 and us-H_2-Fe/SBA-15, were fitted at 298 and 13 K using the same criteria previously described in Section 3.4, for c-CO:H_2-Fe/SBA-15. The spectra and their hyperfine parameters are shown in Fig. 11a and b and in Tables IV and V of Supplementary

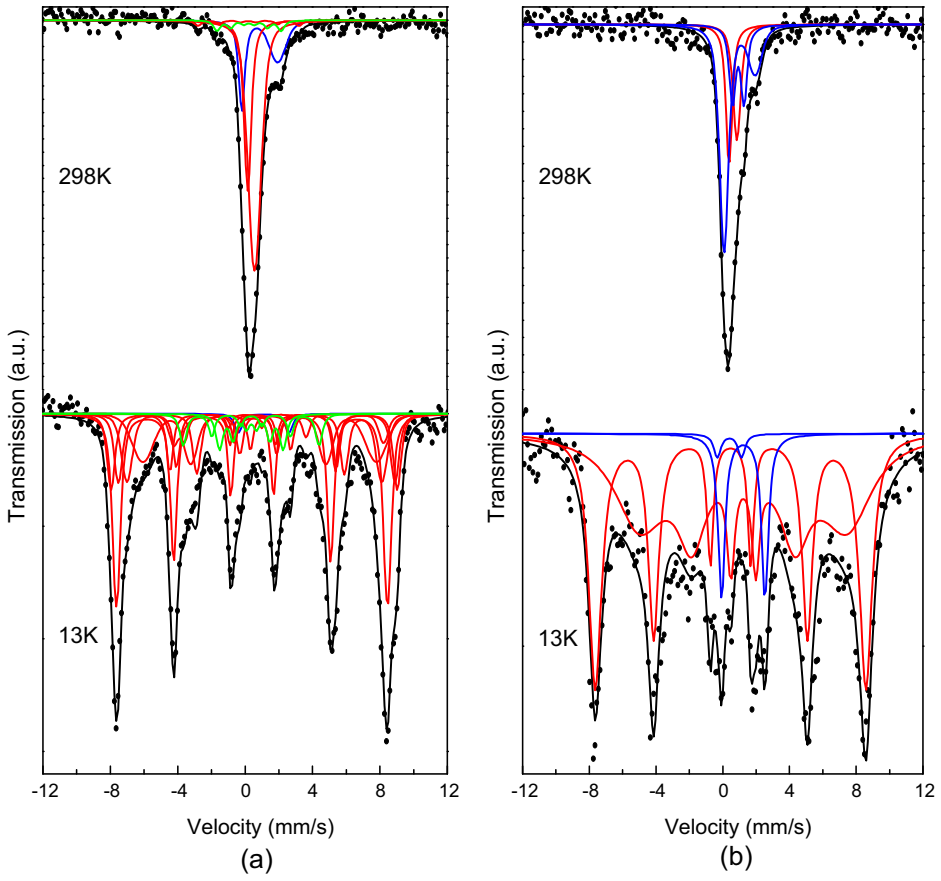

Fig. 10. Mössbauer spectra of activated catalysts at 298 and 13 K measured in controlled atmosphere. (a) c-CO:H_2-Fe/SBA-15 and (b) c-H_2-Fe/SBA-15.

Table 1
Percentage of iron species in c-CO:H_2-Fe/SBA-15, c-H_2-Fe/SBA-15, us-H_2-Fe/SBA-15 and us-CO:H_2-Fe/SBA-15, measured in controlled atmosphere at 13 K.

Species	Activated catalysts		Used catalysts	
	H_2 (%)	H_2:CO (%)	H_2 (%)	H_2:CO (%)
Fe_3O_4	91 ± 7	89 ± 12	64 ± 7	41 ± 5
Fe^{2+}	9 ± 1	1.0 ± 0.1	14 ± 2	45 ± 2
χ-Fe_5C_2 + ε'-$Fe_{2.2}C$	0	10 ± 4	22 ± 7	14 ± 4

Data section. A noticeable difference appears between c-CO:H_2-Fe/SBA-15 and us-CO:H_2-Fe/SBA-15 in the magnetic behavior of Fe_3O_4 at 13 K. In used catalyst, this species has not completed its magnetic blocking at this temperature. As it will be explained in Discussion section, we attributed this result to a breakup of iron carbides "shell", a come up of iron carbides "nodules" and a decreasing of contact area between Fe_3O_4 and surface iron carbides. As a consequence, the exchange anisotropy decreases and a complete magnetic blocking was not achieved.

It is important to remark that the Mössbauer spectra of the used catalysts were measured in the same reaction atmosphere (see experimental section) without air contact. Therefore, the obtained results would represent the structural properties of the "working" catalysts in accurate way. Similar experiments were made by other authors only at 298 K. In the presence of superparamagnetic NPs it is very difficult to obtain conclusions about the present species only with room temperature measurements.

The iron species present were the same in both catalysts, but there are significant differences between their percentages (Table 1). Within the experimental errors the iron carbides quantities are equal in both solids. But there is an important difference between the percentages of Fe^{2+} ions. In the system activated with CO:2H_2 the percentage of this species increases from 1% to 45% during the FTS. In Discussion section a probable explanation to this result will be given.

3.6. Catalytic tests

In order to evaluate whether the structural modifications, generated by the different activation processes, lead to differences in the activity and selectivity results, catalytic tests of the activated solids in different atmospheres were done. In Figs. 12–14 are shown CO conversion, specific velocity of total hydrocarbon production and molar percentage of methane vs. reaction time, respectively. It can be seen that when the "pseudo steady state" has been reached, c-H_2-Fe/SBA-15 has about twice more CO conversion and specific velocity of total hydrocarbon production than c-CO:H_2-Fe/SBA-15. We decided to express the total hydrocarbon production by total iron loading. A more precise way to normalize the total hydrocarbon production requires a measurement of iron surface atoms quantity (e.g. using chemisorption techniques). But it has been determined that the iron species present at zero reaction time change when catalysts are "working". On the other hand, Li et al. [55] proposed a new method to determine the active site density of unsupported iron catalysts using a CO-TPD on the used catalysts. We applied this technique, but in agreement with the results obtained by Xu and Bartholomew [56] with iron supported on silica, our results were unsatisfactory. Perhaps, as it was mentioned by Xu and Bartholomew [56], in FTS conditions both kinds of surface sites able to bond CO by physisorption and chemisorption are active. But, the measurement of the first type of surface sites by CO-TPD method would be negligible, at least

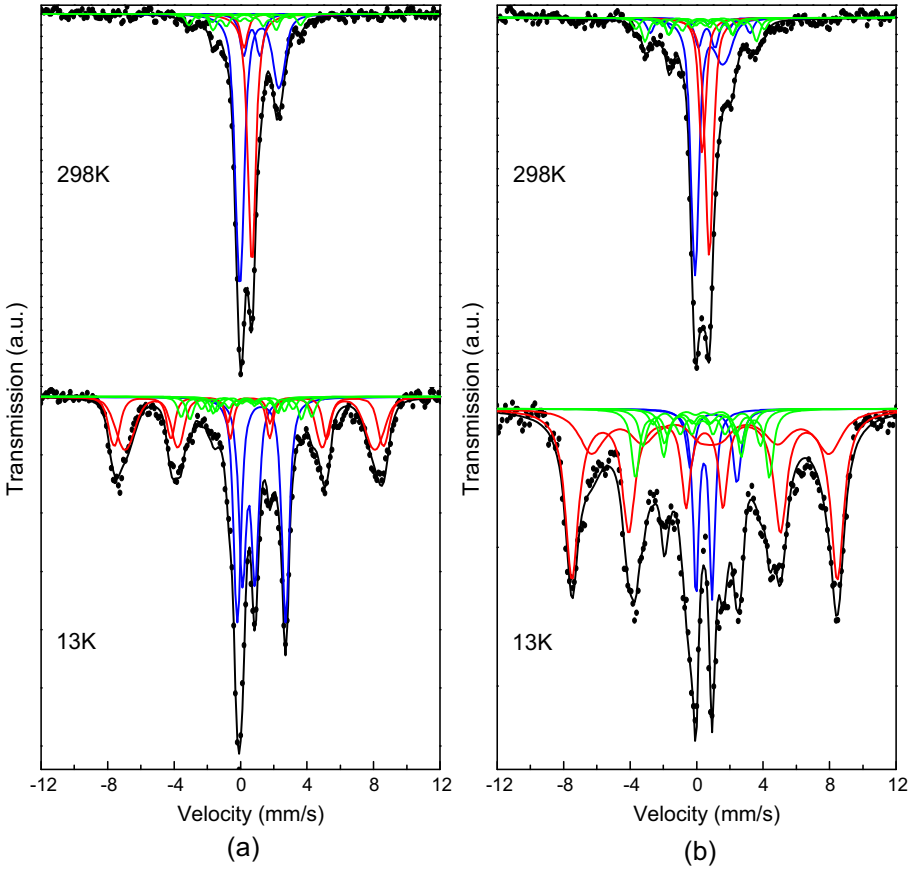

Fig. 11. Mössbauer spectra of used catalysts at 298 and 13 K measured in controlled atmosphere. (a) us-CO:H_2-Fe/SBA-15 and (b) us-H_2-Fe/SBA-15.

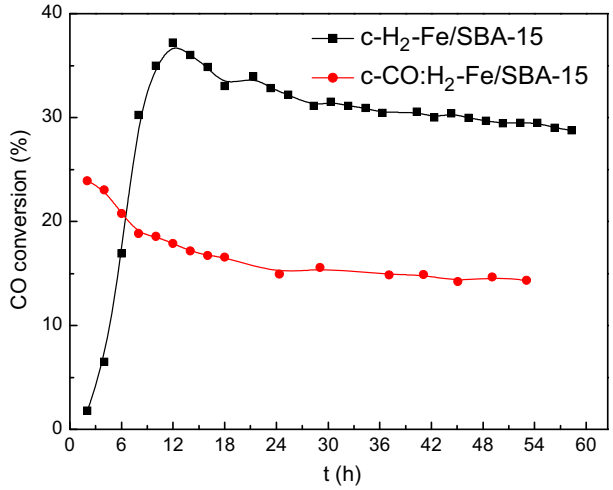

Fig. 12. CO conversion (%) vs. reaction time. Solid lines are to guide the eye only.

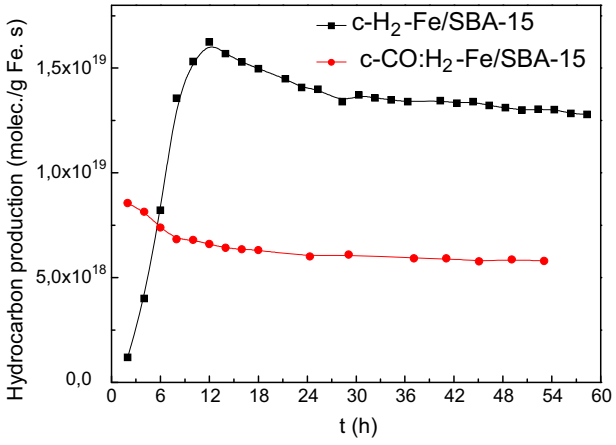

Fig. 13. Specific velocity of total hydrocarbon production (molecules/g Fe s) vs. reaction time. Solid lines are to guide the eye only.

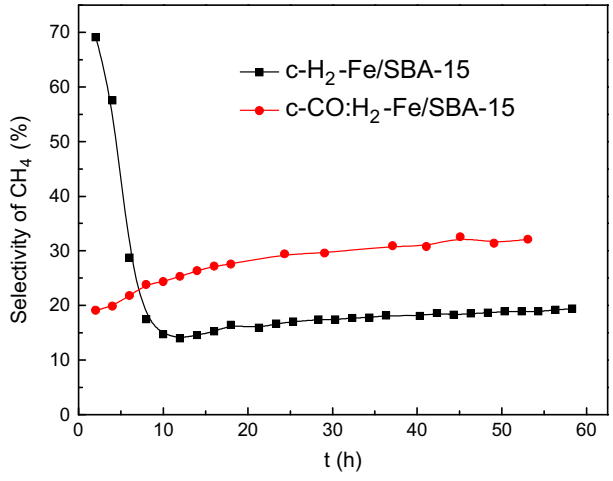

Fig. 14. CH_4 selectivity (%) vs. reaction time. Solid lines are to guide the eye only.

in iron supported systems. Therefore, hitherto there is not an adequate, precise and meaningful method to determine surface iron atoms in reaction conditions. As a consequence we normalized the activity results dividing by iron loading of each catalyst.

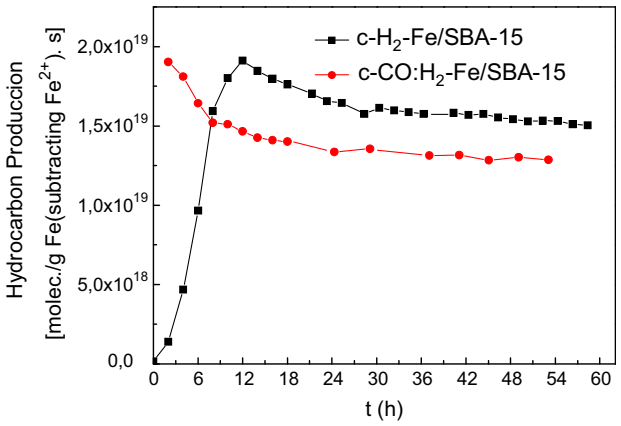

Fig. 15. Specific velocity of total hydrocarbon production subtracting Fe^{2+} content determined by Mössbauer spectroscopy vs. reaction time. Solid lines are to guide the eye only.

Additionally, the catalyst activated in pure H_2, produces 40% less CH_4 (undesirable product in FTS). It is important to remark that the high methane production shown by c-H_2-Fe/SBA-15 in the first minutes of the reaction could be misinterpreted since, a very low conversion is obtained at this time and nearly all molecules produced are of this species. Therefore, the comparison must be realized at the "pseudo steady state".

Taking into account that, Fe^{2+} ions diffused into the SBA-15 walls are inactive in FTS, the activity differences between c-CO:H_2-Fe/SBA-15 and c-H_2-Fe/SBA-15 could be attributed to the higher quantity of this species in c-CO:H_2-Fe/SBA-15. With the aim to check this possibility, we express the specific velocity of total hydrocarbon production subtracting this species. The results obtained are shown in Fig. 15. After this normalization, c-H_2-Fe/SBA-15 has an activity of about 20% higher than that showed by c-CO:H_2-Fe/SBA-15. Therefore, it can be concluded that the higher activity of c-H_2-Fe/SBA-15 is an authentic result.

Both catalysts display an excellent stability with the reaction time. Taking into account that both precursors are identical, these results demonstrate the importance of the correct choice of the activation atmosphere in order to reach more active and selective catalysts for FTS.

4. Discussion

In order to explain the activity differences produced by different activation atmospheres it is necessary to analyze the bibliography related to the active sites in FTS. As it was mentioned previously, their nature is elusive up to date. However, the current literature would indicate that the C necessary to produce hydrocarbons "gets away" from the carbide surfaces. As a consequence, surface empty sites appear and they enhance CO adsorption and CO dissociation energy barrier largely decreases. Therefore, the vacancies are refilled with new CO molecules that are dissociated, and the active carbide surface is regenerated. These conclusions were obtained recently by theoretical calculus [57,58] and were reinforced with experimental results on iron supported on SBA-15 systems [59]. In Cano et al. [59] a detailed description of this model, combining previous finding of the aforementioned researches [57,58] with their own results, was shown.

Previous results have showed that, in Fe bulk catalysts, iron carbides grow on the surface of iron oxides as superficial "nodules" [12]. We assume that this mechanism is maintained with supported iron oxides NPs.

Bearing in mind this premise, we could describe the activation step and catalytic "work" of the system in the following way:

- if the activation is realized with CO:H_2, a simultaneous process of reduction/carburization of γ-Fe_2O_3 is produced. This situation could be described using a "shrinking-core" model. Assuming this oversimplified description, each NP would have a "core" of maghemite and two "shells": the inner of Fe_3O_4 and the outer of iron carbides at zero reaction time. The progress of both "shells" would be controlled by the diffusion of oxygen species from γ-Fe_2O_3 to NPs surface. When these "shells" have growth enough, a breakup of the carbide "shell" would occur in order to accommodate the density mismatch between oxide and carbide phases and the iron carbide "nodules" would appear on the NPs surface [55],
- instead, when the catalyst is activated with pure H_2, pure Fe_3O_4 NPs are suddenly placed in contact with CO:H_2 mixture at the beginning of the reaction. Now, the diffusion of oxygen species does not control the total process. Therefore, the production of iron carbides nuclei on NPs surface would occur very quickly. As a consequence, would appear a greater number of iron carbides surface "nodules" in comparison with those that would be produced when CO:H_2 activation atmosphere is used. Besides, these "nodules" would have a lower size. Therefore, a larger number of sites for CO adsorption and dissociation and shorter diffusion paths would be obtained when pure H_2 is used in the activation treatment instead of H_2:CO and the catalyst will be more active. As it was previously mentioned, the effect remains if the quantity of Fe^{2+} ions (diffused inside the SBA-15 walls) is subtracted (Fig. 15). Besides, there is another experimental result that can be observed in Table 1: in the "working" catalysts the ratios $Fe_3O_4/(\chi\text{-}Fe_5C_2 + \varepsilon'\text{-}Fe_{2.2}C)$ – after subtract Fe^{2+} content – are identical: 2.8. Therefore, the distinct catalytic results would be attributed to NPs structural differences produced by different activation treatments instead of different species and/or quantities of them. The present activity results can be justified using this description. In Fig. 16 a schematic representation of these steps using the proposed model is shown.

From this model, it would be possible to explain the different percentages of Fe^{2+} ions diffused inside the SBA-15 walls when the activation atmosphere was changed. We link this effect with the "wetting" of the active species on the support. Thus, the contact angle (θ) between two phases is defined by Young's equation:

$$\gamma_{ag}\cos\theta = \gamma_{sg} - \gamma_{as} \quad (1)$$

where γ values are the specific interface free energies between phases "i" and "j". The means of "a", "s" and "g" are active phase, support and gas phases respectively [60]. Under equilibrium conditions, when $\theta > 90°$ the active phase does not "wet" the support. Instead, when $\theta < 90°$, the "wetting" occurs [61]. Applying Young's equation to our systems, after activation process and before the beginning of FTS, we have the following:

CO:H_2 activation atmosphere:

$$\cos\theta_{CO:H2} = \frac{\gamma_{SBA15/CO:H2} - \gamma_{Fe3O4/SBA15}}{\gamma_{\text{iron carbides/CO:H2}}} \quad (2)$$

H_2 activation atmosphere:

$$\cos\theta_{H2} = \frac{\gamma_{SBA15/H2} - \gamma_{Fe3O4/SBA15}}{\gamma_{Fe3O4/H2}} \quad (3)$$

In Eq. (2) Fe_3O_4 has been considered the iron active phase in contact with the support. Considering negligible differences between $\gamma_{SBA15/CO:H2}$ and $\gamma_{SBA15/H2}$ (they have the same support) the following ratio can be established:

$$\frac{\cos\theta_{CO:H2}}{\cos\theta_{H2}} = \frac{\gamma_{Fe3O4/H2}}{\gamma_{\text{iron carbides/CO:H2}}} \quad (4)$$

Taking into account the structural similarities between alpha-iron and iron carbides, very similar values of $\gamma_{iron/gas}$ and $\gamma_{\text{iron carbides/gas}}$ could be expected. On the other hand, $\gamma_{\text{iron oxides/gas}}$ value is about five times lower [60,61]. Therefore, we can deduce that when CO:H_2 is used as activation atmosphere, the surface of the NPs changes from iron oxide to iron carbides, and the angle between iron carbides "shell" and SBA-15 is considerably decreased [Fig. 16]. Thus, the contact area between NPs/SBA-15 is increased. As a

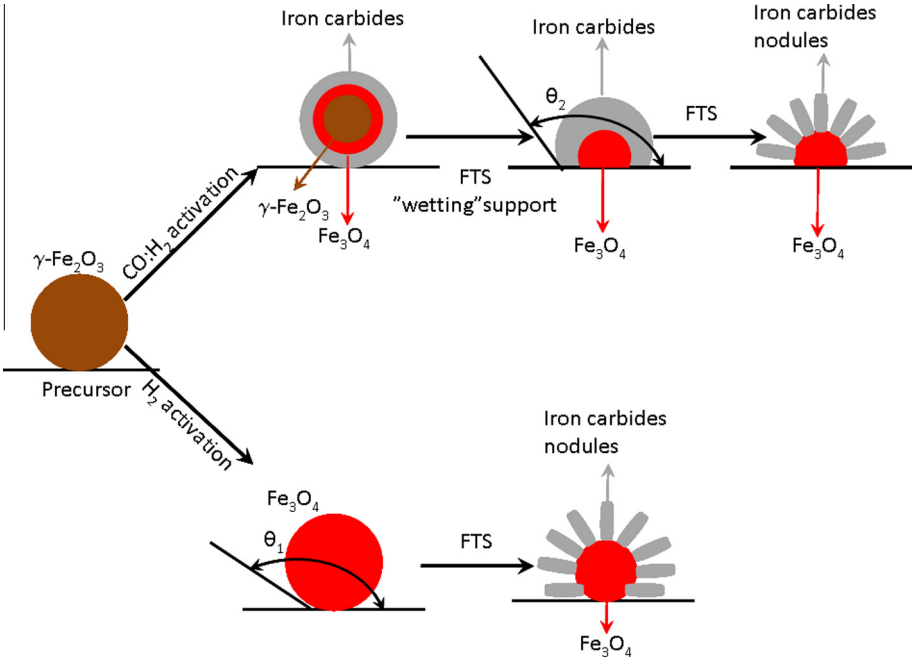

Fig. 16. Schematic representation of sequential phase modifications from precursor up to "working" catalysts depending on the activation atmospheres. Also, the effect of different "wetting" of support is considered. Note that $\theta_1 > \theta_2$.

consequence, the diffusion probability of Fe^{2+} ions inside the SBA-15 walls is incremented. This rough model explains the experimental results obtained by Mössbauer technique.

5. Conclusions

A significant influence of the activation atmosphere on the activity and selectivity in FTS using iron supported catalysts has been shown in the present work. In order to establish this conclusion, many structural properties must be controlled. Thus, particle sizes of the active phase and size and shape of support pores, must be carefully controlled in order to avoid secondary effects such as presence of "structure sensitivity", diffusional control and shape selectivity. To overcome these difficulties, we carried out a new strategy with the aim to obtain a catalytic solid "tailor-made". In this way, γ-Fe_2O_3 NPs of 3 nm were pre-synthesized and located inside the channels of mesoporous SBA-15. We named these solids "quasi model" catalysts. The NPs and catalysts were precisely characterized by different techniques, then, were activated in CO:H_2 or pure H_2 and catalytically tested in the FTS at 20 atm. The experimental results showed that activation with pure H_2 produces a catalyst more active and less selective to methane. In order to explain these results, we proposed different reduction sequences depending on the mechanism of species generation. Activation in H_2:CO would occur following a "shrinking-core" model. Instead, pure H_2 would lead to expose suddenly the NPs surface of Fe_3O_4 to a carburizing mix (H_2:CO). This situation would produce a great number of iron carbide nuclei. The NPs in the "working" catalysts would have great number of iron carbide "nodules" with smaller size if pure H_2 is used as activation atmosphere. Therefore, a larger number of sites for CO adsorption and dissociation and shorter diffusion paths would be obtained and the catalyst will be more active.

Besides, making use of this general picture and adding interface free energies concepts, we explain the possible origin of a greater percentage of Fe^{2+} ions diffused inside the SBA-15 walls when CO:H_2 activation atmosphere is used.

Acknowledgments

The authors acknowledge the financial support of ANPCyT (PICT N° 0340) and CONICET (PIP N° 00547) which allowed the development of this work. We wish to thank Dr. S. Figueroa who did small angle XRD diffractograms.

Appendix A. Supplementary material

Supplementary data associated with this article can be found, in the online version, at http://dx.doi.org/10.1016/j.jcat.2015.12.004.

References

[1] A. Steynberg, M. Dry (Eds.), Fischer–Tropsch Technology, Stud. Surf. Sci. Catal., Elsevier, 2004.
[2] B.H. Davis, M.L. Occelli (Eds.), Fischer–Tropsch Synthesis, Catalysts and Catalysis, Stud. Surf. Sci. Catal., Elsevier, 2007.
[3] M. Luo, H. Hamdeh, B.H. Davis, Catal. Today 140 (2009) 127.
[4] R.B. Anderson, in: P.H. Emmett (Ed.), Catalysis, IV, Reinhold, New York, 1956.
[5] R.B. Anderson, The Fischer–Tropsch Synthesis, Academic Press, Orlando, FL, 1984.
[6] J.A. Amelse, J.B. Butt, L.H. Schwartz, J. Phys. Chem. 82 (1978) 558.
[7] G.B. Raupp, W.N. Delgass, J. Catal. 58 (1979) 361.
[8] J.W. Niemantsverdriet, A.M. van der Kraan, J. Catal. 72 (1981) 385.
[9] J.P. Reymond, P. Meriadeau, S.J. Teichner, J. Catal. 75 (1982) 39.
[10] F. Blanchard, J.P. Reymond, B. Pommier, S.J. Teichner, J. Mol. Catal. 17 (1982) 171.
[11] R. Dictor, A.T. Bell, J. Catal. 97 (1986) 121.
[12] M.D. Shroff, D.S. Kalakkad, K.E. Coulter, S.D. Köhler, M.S. Harrington, N.B. Jackson, A.G. Sault, A.K. Datye, J. Catal. 156 (1995) 185.
[13] S. Soled, E. Iglesia, R.A. Fiato, Catal. Lett. 7 (1990) 271.
[14] C.S. Kuivila, P.C. Stair, J.B. Butt, J. Catal. 118 (1989) 299.
[15] J.B. Butt, Catal. Lett. 7 (1990) 61.
[16] H.W. Pennline, M.F. Zarochak, J.M. Stencel, J.R. Diehl, Ind. Eng. Chem. Res. 26 (1987) 595.
[17] D.B. Bukur, L. Nowicki, R.K. Manne, X. Lang, J. Catal. 155 (1995) 366.
[18] D.B. Bukur, L. Nowicki, X. Lang, Catal. Today 24 (1995) 111.
[19] R.J. O'Brien, L. Xu, R.L. Spicer, B.H. Davis, Energy Fuels 10 (1996) 921.
[20] R.J. O'Brien, L. Xu, R.L. Spicer, S. Bao, D.R. Milburn, B.H. Davis, Catal. Today 36 (1997) 325.
[21] M. Boudart, A. Delbouille, J.A. Dumesic, S. Khammouma, H. Topsøe, J. Catal. 37 (1975) 486.
[22] M.A. McDonald, D.A. Storm, M. Boudart, J. Catal. 102 (1986) 386.
[23] E.I. Mabaso, E. van Steen, M. Claeys, DGMK, Tagungsbericht 4 (2006) 93.
[24] L.A. Cano, M.V. Cagnoli, N.A. Fellenz, J.F. Bengoa, N.G. Gallegos, A.M. Alvarez, S. G. Marchetti, Appl. Catal., A 379 (2010) 105.
[25] H.-J. Freund, Surf. Sci. 601 (2007) 1438.
[26] S. Sun, H. Zeng, D.B. Robinson, S. Raoux, P.M. Rice, S.X. Wang, G. Li, J. Am. Chem. Soc. 126 (1) (2004) 273.
[27] I.O. Perez De Berti, M.V. Cagnoli, G. Pecchi, J.L. Alessandrini, S.J. Stewart, J.F. Bengoa, S.G. Marchetti, Nanotechnology 24 (2013) 175601.
[28] D. Zhao, J. Feng, Q. Huo, N. Melosh, G.H. Fredrickson, B.F. Chmelka, G.D. Stucky, Science 279 (1998) 23.
[29] D. Zhao, Q. Huo, J. Feng, B.F. Chmelka, G.D. Stucky, J. Am. Chem. Soc. 120 (1998) 6024.
[30] E.I. Mabaso, E. van Steen, M. Claeys, Fischer–Tropsch synthesis on supported iron crystallites of different size, in: Proc. DGMK/SCI-Conference, Dresden, Germany, October 4–6, 2006.
[31] D. Barkhuizen, I. Mabaso, E. Viljoen, C. Welker, M. Claeys, E. van Steen, J.C.Q. Fletcher, Pure Appl. Chem. 78 (9) (2006) 1759.
[32] J.-Y. Park, Y.-J. Lee, P.K. Khanna, K.-W. Jun, J.W. Bae, Y.H. Kim, J. Mol. Catal. A: Chem. 323 (2010) 84.
[33] L. Cao, T. Man, M. Kruk, Chem. Mater. 21 (2009) 1144.
[34] W.K. Jozwiak, E. Kaczmarek, T.P. Maniecki, W. Ignaczak, W. Maniukiewicz, Appl. Catal., A: General 326 (2007) 17–27.
[35] I. Pérez De Berti, J. Bengoa, N. Fellenz, R. Mercader, S. Marchetti, Rev. Sci. Instrum. 86 (2015) 023903.
[36] D.C. Harris, Quantitative Chemical Analysis, fifth ed., W.H. Freeman & Co, New York, USA, 1998.
[37] K. Lagarec, D.G. Rancourt, Mossbauer Spectral Analysis Software, Dep. of Phys., University of Ottawa, Version 1.0., 1998.
[38] C.G. Granqvist, R.A. Buhrman, J. Appl. Phys. 47 (1976) 2200.
[39] E. Murad, Hyperfine Interact. 117 (1998) 39.
[40] Y. Komorida, M. Mito, H. Deguchi, S. Takagi, A. Millán, N.J.O. Silva, F. Palacio, Appl. Phys. Lett. 94 (2009) 202503.
[41] L.M. Bronstein, X. Huang, J. Retrum, A. Schmucker, M. Pink, B.D. Stein, B. Dragnea, Chem. Mater. 19 (2007) 3624.
[42] M.M. Lin, D.K. Kim, J. Nanopart. Res. 14 (2012) 688.
[43] N. Feltin, M.P. Pileni, Langmuir 13 (1997) 3927.
[44] J.M.D. Coey, Phys. Rev. Lett. 27 (1971) 1140.
[45] D. Peddis, M.V. Mansilla, S. Mørup, C. Cannas, A. Musinu, G. Piccaluga, F. D'Orazio, F. Lucari, D. Fiorani, J. Phys. Chem. B 112 (2008) 8507.
[46] L. Del Bianco, D. Fiorani, A.M. Testa, E. Bonetti, L. Savini, S. Signoretti, Phys. Rev. B 66 (2002) 174418.
[47] D.G. Rancourt, J.M. Daniels, Phys. Rev. B 29 (5) (1984) 2410.
[48] B.S. Clausen, H. Topsøe, S. Mørup, Appl. Catal. 48 (1989) 327.
[49] S.Ch. Lin, J. Phillips, J. Appl. Phys. 58 (5) (1943) 1985.
[50] A. Meffre, B. Mehdaoui, V. Kelsen, P.F. Fazzini, J. Carrey, S. Lachaize, M. Respaud, B. Chaudret, Nano Lett. 12 (2012) 4722.
[51] I. Dézsi, Cs. Fetzer, Á. Gombkötő, I. Szűcs, J. Gubicza, T. Ungár, J. Appl. Phys. 103 (2008) 104312.
[52] M. Pijolat, V. Perrichon, P. Bussiére, J. Catal. 107 (1987) 82.
[53] S. Mórup, J.A. Dumesic, H. Topsøe, in: R.L. Cohen (Ed.), Applications of Mössbauer Spectroscopy, vol. II, Academic Press, New York, 1980. p. 1.
[54] S. Mørup, in: H. Kronmüller, S. Parkin (Eds.), Handbook of Magnetism and Advanced Magnetic Materials, vol. IV, John Wiley & Sons, Ltd., Chichester, UK, 2007.
[55] S. Li, W. Ding, G.D. Meitzner, E.J. Iglesia, Phys. Chem. B 106 (2002) 85.
[56] J. Xu, C.H. Bartholomew, J. Phys. Chem. B 109 (2005) 2392.
[57] Ch.-F. Huo, Y.-W. Li, J. Wang, H. Jiao, J. Am. Chem. Soc. 131 (2009) 14713.
[58] J.M. Gracia, F.F. Prinsloo, J.W. Niemantsverdriet, Catal. Lett. 133 (2009) 257.
[59] L.A. Cano, M.V. Cagnoli, J.F. Bengoa, A.M. Alvarez, S.G. Marchetti, J. Catal. 278 (2011) 310.
[60] H. Knözinger, E. Taglauer, in: G. Ertl, H. Knözinger, J. Weitkamp (Eds.), Handbook of Heterogeneous Catalysis, VCH A Wiley Company, 1997. p. 216.
[61] S.H. Overbury, P.A. Bertrand, G.A. Somorjai, Chem. Rev. 75 (5) (1975) 547.